

Current Biology, Volume 30

## Supplemental Information

**Input Connectivity Reveals Additional**

**Heterogeneity of Dopaminergic**

**Reinforcement in *Drosophila***

**Nils Otto, Markus W. Pleijzier, Isabel C. Morgan, Amelia J. Edmondson-Stait, Konrad J. Heinz, Ildiko Stark, Georgia Dempsey, Masayoshi Ito, Ishaan Kapoor, Joseph Hsu, Philipp M. Schlegel, Alexander S. Bates, Li Feng, Marta Costa, Kei Ito, Davi D. Bock, Gerald M. Rubin, Gregory S.X.E. Jefferis, and Scott Waddell**

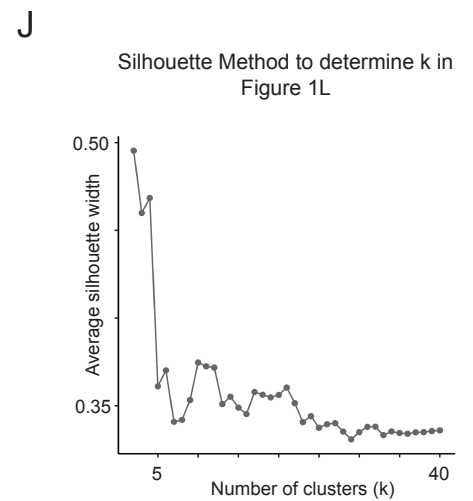
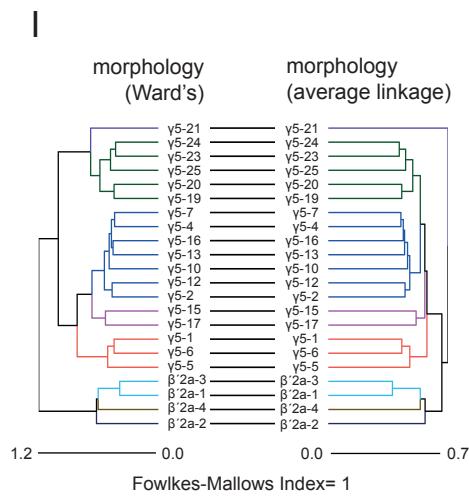
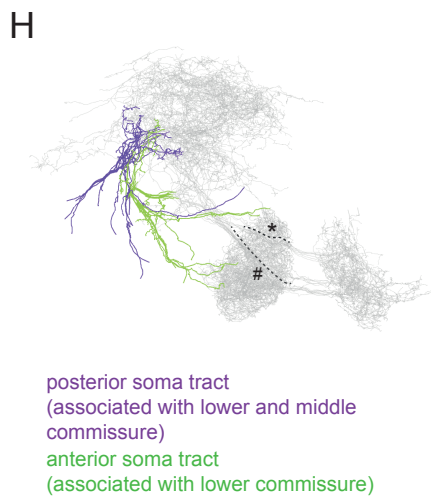
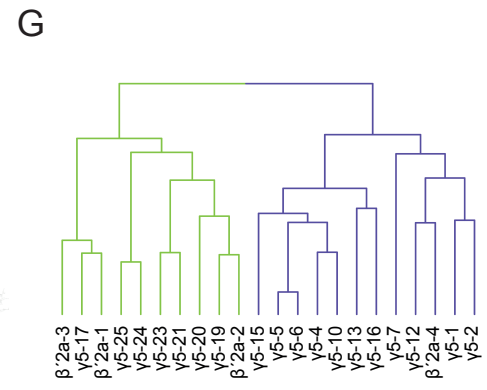
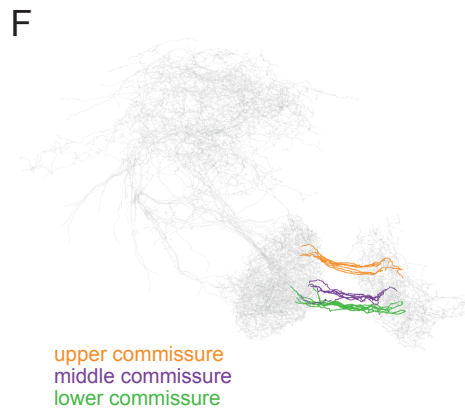
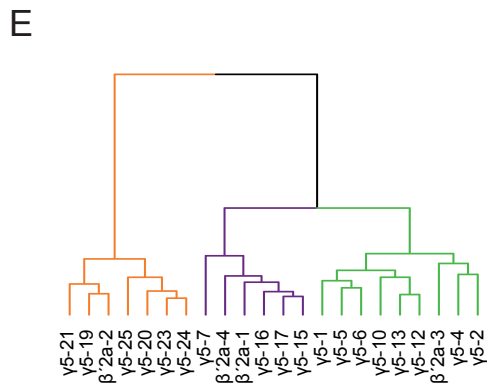
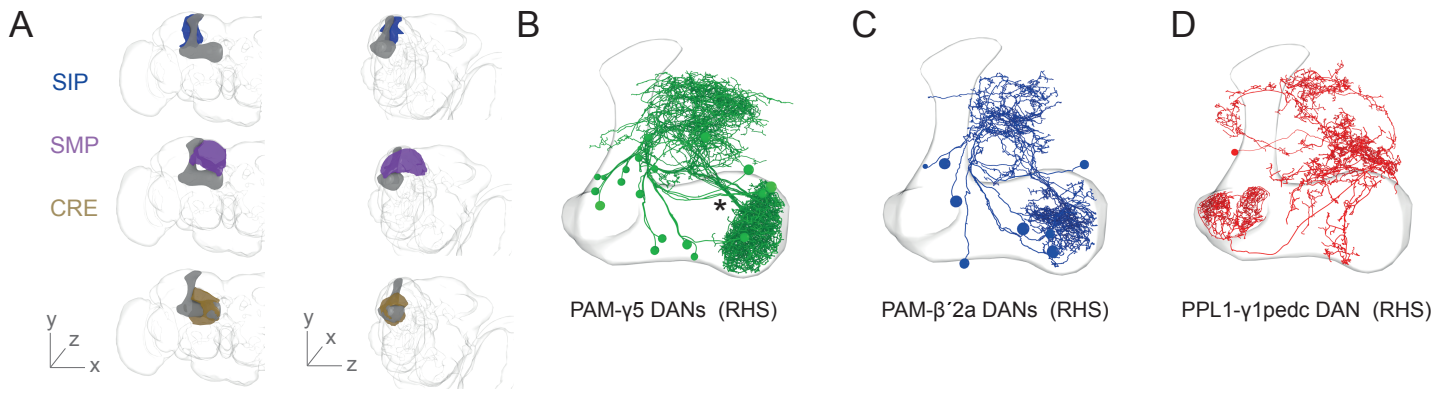


### Figure S1 related to Figure 1

(A) Areas of neuropil providing most input to the DANs in this study as defined in CATMAID and named according to [17]. The superior medial protocerebrum (SMP, purple), superior intermediate protocerebrum (SIP, blue) and crepine (CRE, ochre) are shown from the front (left) and from the midline (right). The MB and whole brain neuropil are depicted in grey. (B-D) Representations of all reviewed DANs in the fly's right hemisphere. (B) 20 PAM- $\gamma$ 5 DANs. MB outlined, asterisk indicates 2 descending soma tracts. (C) 8 confirmed PAM- $\beta$ '2a DAN candidates. (D) PPL1-  $\gamma$ 1pedc DAN with elaborate dendrite outside the MB. (E) Dendrogram using only the commissure part of the PAM- $\gamma$ 5 and PAM- $\beta$ '2a DANs reveals 3 morphological clusters. (F) Projection view of the upper (orange), middle (purple) and lower (green) commissure DAN groups from the clustering in (E). Full DAN morphologies are shown in grey. (G) Average linkage clustering using the tracts connecting the somata and dendrites reveals 2 distinct groups. (H) Projection view of the posterior (purple) and anterior (green) soma tracts from clustering in (G). The posterior tract mostly contains lower commissure DANs (dashed line and hash) whereas the anterior tract mostly houses upper commissure DANs (dashed line and asterisk). (I) Tanglegram illustrating comparison of morphological clustering obtained using average linkage criterion (as in Figure 1B) to that retrieved using Ward's criterion. The clusters are identical, hence Fowlkes-Mallows Index is 1. Note: the between cluster relationship varies slightly. (J) Silhouette method to determine the appropriate number of clusters (k) selected for Ward's criterion based hierarchical clustering of 3-dimensional positions of PPL1- $\gamma$ 1pedc post synapses. Accuracy drops after 4 clusters and k=4 best reflects the quadripartite structure of the PPL1- $\gamma$ 1pedc dendrite.

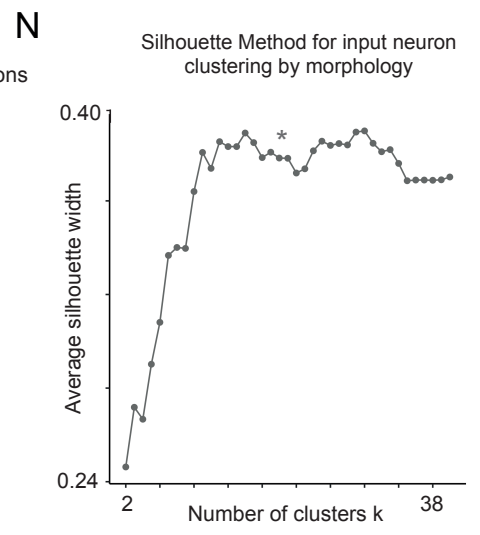
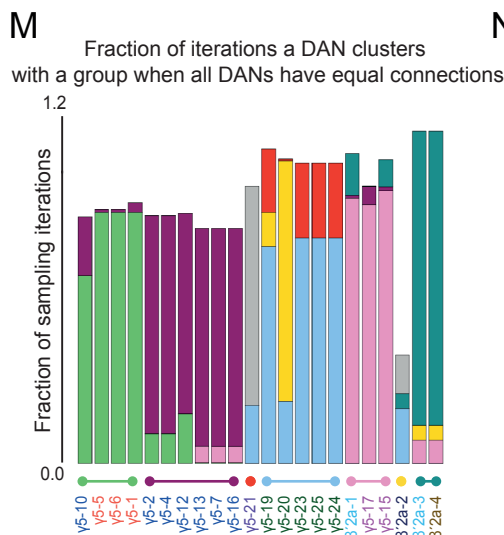
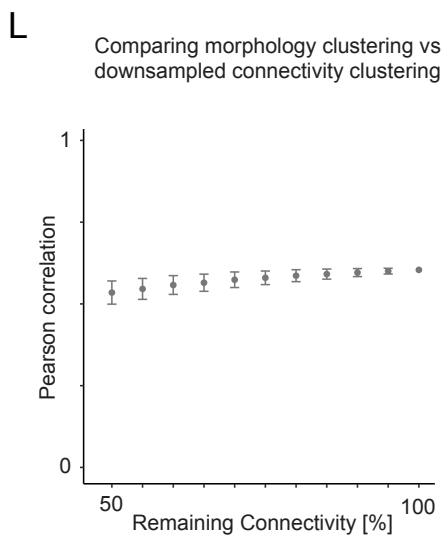
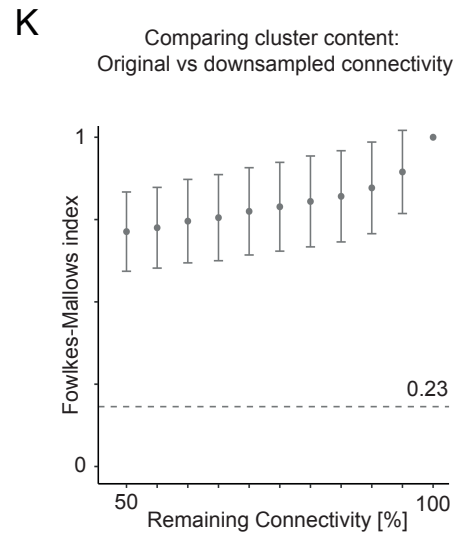
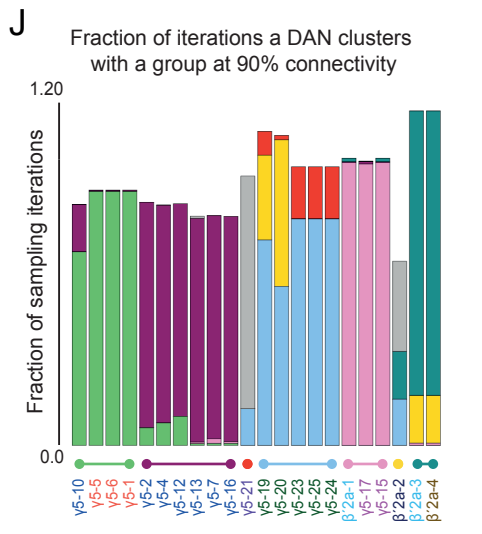
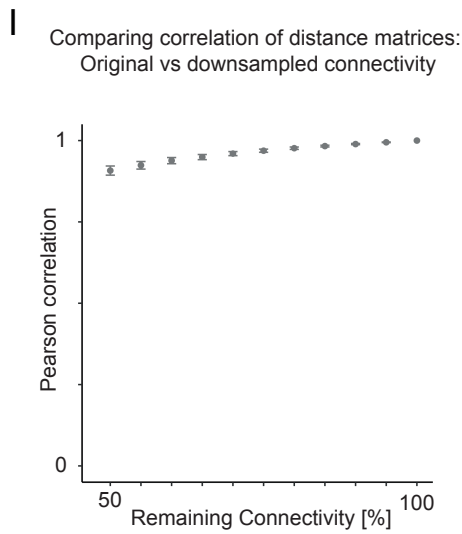
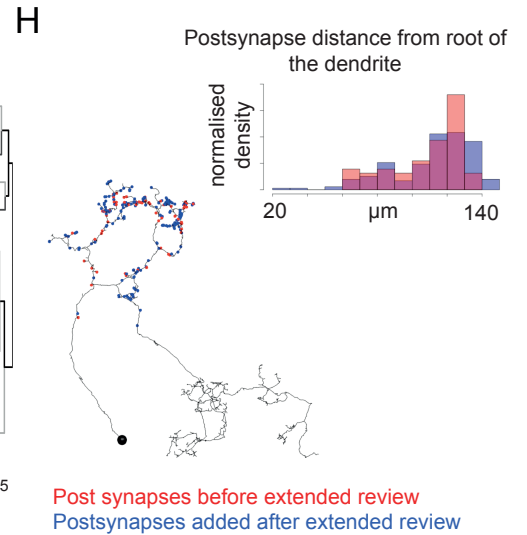
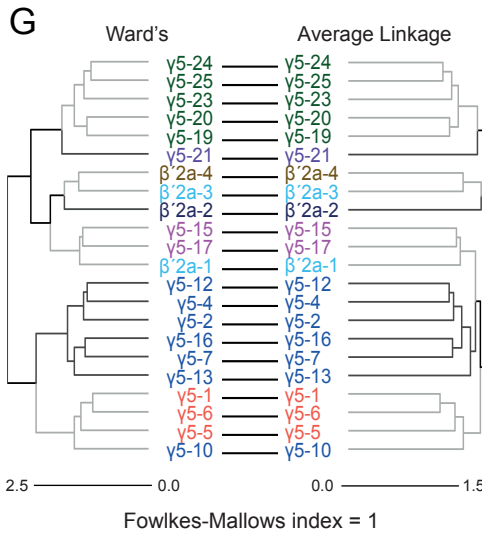
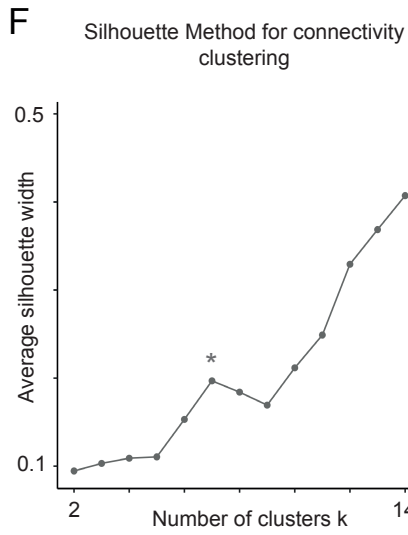
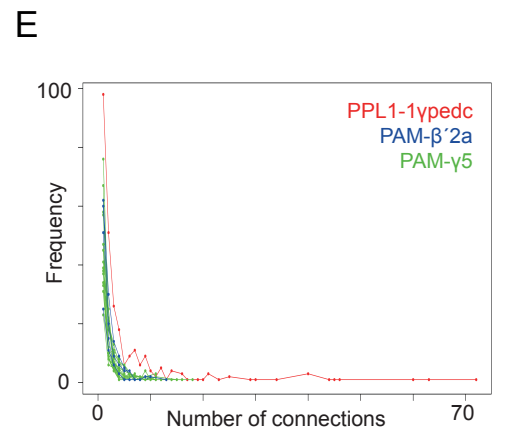
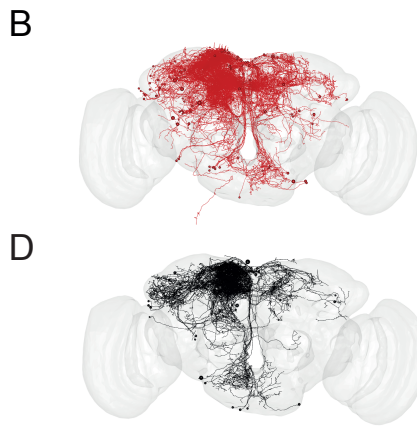
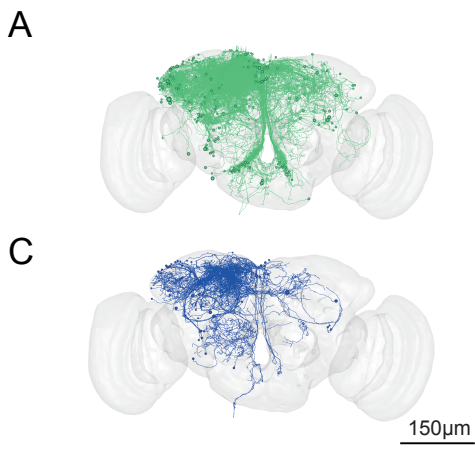
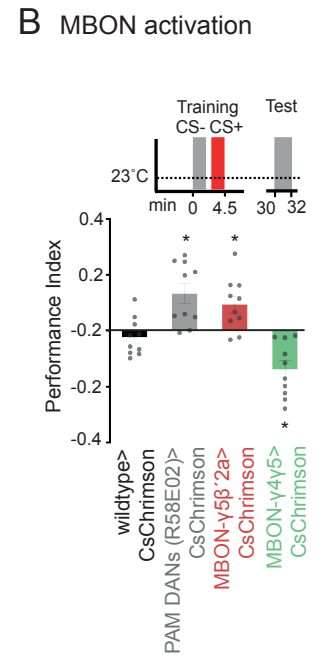
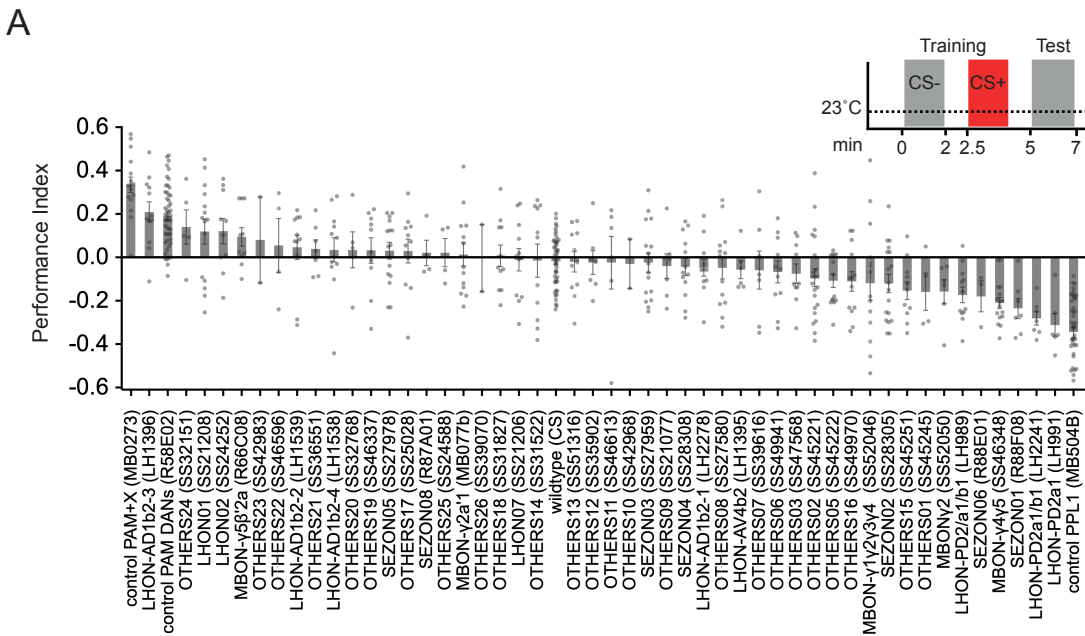




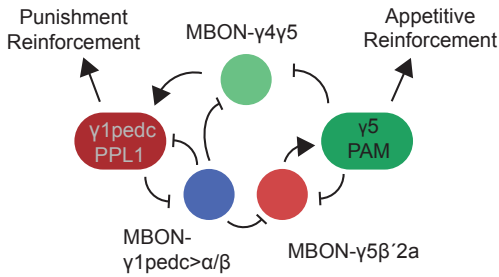
**Figure S2. DAN clustering by input connectivity is reproducible with different algorithms and is not generated by tracing bias, related to Figure 2.**

(A-D) Related to Figures 2C and 2G. Representation of input neurons unique to (A) PAM- $\gamma$ 5 DANs (green), (B) PPL1- $\gamma$ 1pedc (red) and (C) PAM- $\beta$ '2a DANs (blue). (D) Shared inputs (black). Whole brain outlined in grey. (E) Related to Figure 2D. Absolute (non-normalised) edge weight distribution between input neurons and DANs. The frequency at which an input to a given DAN with a certain number of connections occurs is shown as a function of the number of connections. DANs receive many inputs connected with only one or few synapses (skew to left). The long tailed distribution of PPL1- $\gamma$ 1pedc indicates it has some inputs with high absolute edge weights. (F) The Silhouette method was used to determine the appropriate cluster number ( $k$ ) for connectivity clustering using Ward's criterion. Due to the high number of unique inputs with low connection number (Figure S2E), a single cluster for each DAN would be optimal. We chose  $k=7$  to reflect the number of morphological DAN subclusters and the local maximum at 7 (asterisk) suggests  $k=7$  is accurate. (G) Tanglegram illustrating comparison of connectivity clustering using Ward's criterion versus that from average linkage criterion. Identical clusters are formed although the between cluster relationship varies slightly. (H) Comparison of localization of postsynapses created by additional extensive review cycles compared to those identified following normal expert review. Marking the synapses along a  $\gamma$ 5 DAN dendrite suggests both classes of synapses to be uniformly distributed. Plotting the distribution of synapses by measuring their positions as distance to the root of the dendritic tree confirms that both the standard and extensively reviewed populations are mixed along the dendrite. These analyses indicate that traced neurons that have undergone standard expert review, but not subjected to extensive review, can be considered to be randomly sampled. (I – L) To test whether input clustering is biased by an incompletely traced input network, we randomly down-sampled the connectivity dataset from 95% – 50% connectivity and compared the clustering obtained from these simulated datasets to the observed connectivity dataset (defined as 100% connectivity). (I) Plot illustrating correlation of connectivity distance matrices for differently down-sampled datasets versus our starting 100% connectivity dataset. Data are mean  $\pm$  standard deviation (SD). The Pearson's correlation remains  $>0.9$  even at 50% downsampling. The Null model based on randomised cluster allocation has a correlation of  $4 \times 10^{-4}$ . (J) To determine whether the DANs cluster in the same groups in the reduced (90%) connectivity dataset we compared their distributions in 10,000 iterations to those in the observed clusters at 100% connectivity. The fraction of times each neuron clusters

with a particular group is shown, color coded according to the observed connectivity groups in Figure 2H (Also see cluster similarity analyses in Materials and Methods). Most DANs are reproducibly cluster with the same groups at 90% connectivity and only the  $\gamma$ 5-19,  $\gamma$ 5-20 and  $\beta$ '2a-2 show any propensity (<40%) to cluster with a different group. (K) The differences in clustering for 10,000 down-sampled datasets at each connectivity density can be individually compared to the observed 100% connectivity dataset using the Fowlkes-Mallows index (FMI). Even 50% connectivity datasets have an FMI (average = 0.71) well above the comparison for a randomised cluster allocation – the null model, Data are mean +/- SD, FMI = 0.21. (L) Pearson's Correlation between connectivity and morphology for 100% and down-sampled connectivity datasets shows only subtle changes even at 50% connectivity, indicating that changes in (k) do not greatly alter the correlation between morphological and connectivity groups. (Randomised cluster allocation null model:  $-6 \times 10^{-4}$ ). Data are mean +/- SD. (M) To test whether input connectivity clustering results were biased by the varying completeness of DAN post synapse annotation cluster similarity analyses were performed on 10,000 datasets in which all extensively reviewed PAM DANs had their connectivity (on average 216 inputs) down-sampled to the average connectivity of normally reviewed PAM DANs (on average 123 inputs). Only The  $\gamma$ 5-20 and  $\beta$ '2a-2 DANs vary in their grouping with  $\beta$ '2a-2 likely to cluster with the  $\gamma$ 5(uc) DANs and  $\gamma$ 5-20 clustering alone. Clustering of all other DANs is stable indicating that the conclusions of this study do not result from biased completeness of tracing. (N) The Silhouette method was used to determine the accuracy of (k) for clustering based on input structure. Beyond 10 clusters the average silhouette width is high so taken with evaluation of cell body locations  $k = 20$  was deemed to be accurate.



**C Previous experience reinforcement**



**D Genotypes used in E-H**

- 1 wildtype >
  - 2 PAM (R58E02) >
  - 3 SEZON01 >
  - 4 SEZON02 >
  - 5 SEZON03 >
  - 6 PPL1-γ1pedc > (MB320C)
- a *Sh<sup>1s1</sup>*
- b *wildtype*

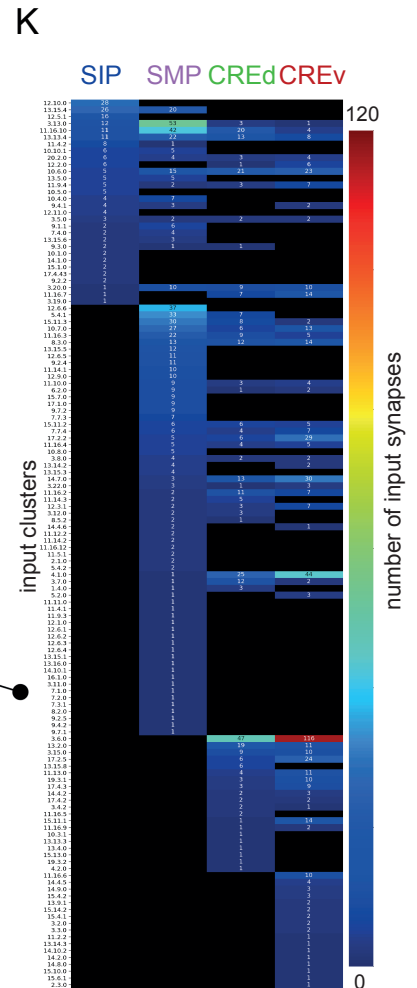
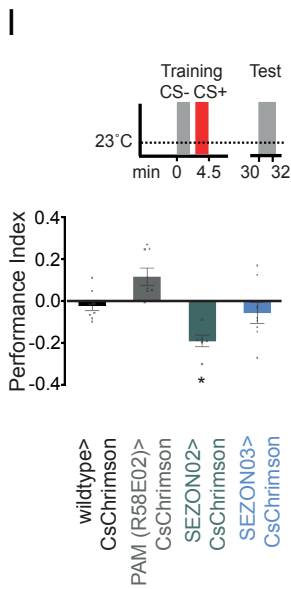
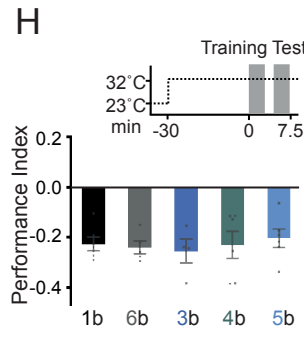
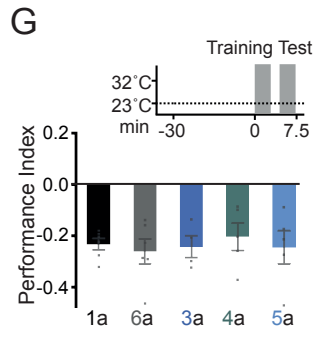
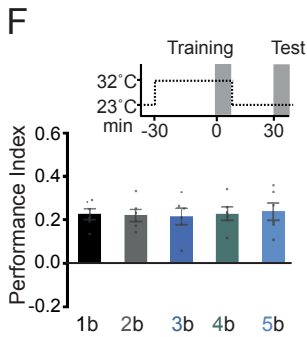
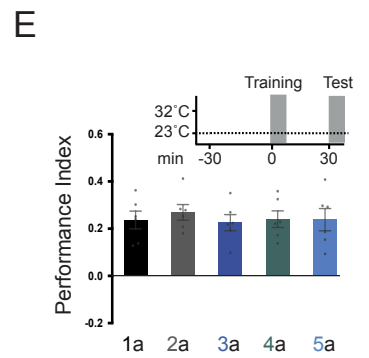
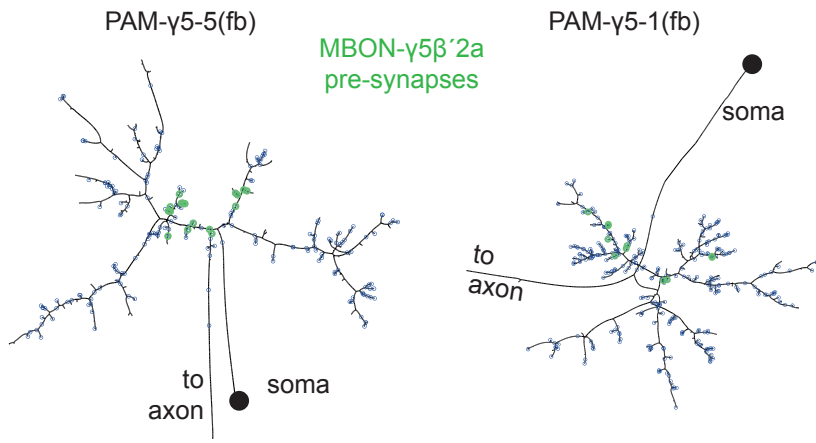


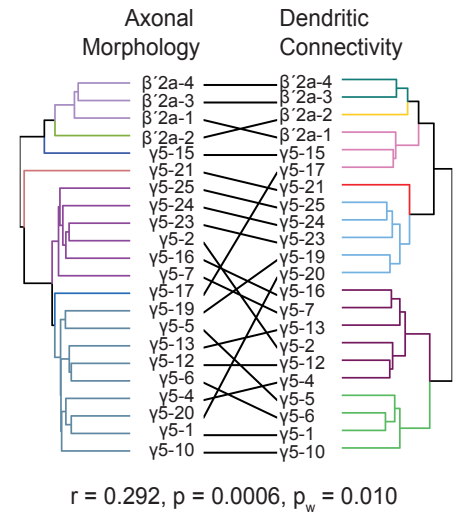
**Figure S3. Functional analyses of DAN input neurons, related to Figure 3.**

(A) Detail of screening results in Figure 3A. Data in all panels are mean  $\pm$  SEM, individual data points are displayed as dots. (B) MBON activation paired with odor exposure can write memories. Following identification in the screen, MBON- $\gamma 5\beta'2a$  and MBON- $\gamma 4\gamma 5$  were retested with 30 min memory being assessed. Activation of MBON- $\gamma 5\beta'2a$  formed weak positive memory ( $p < 0.0247$ ), whereas MBON- $\gamma 4\gamma 5$  activation formed aversive memory ( $p < 0.026$ ). PAM DANs ( $p < 0.0021$ ) (PAM DANs). Asterisks denote significance, one-way ANOVA, with Dunnett's post hoc test for multiple comparisons,  $n = 10$ . (C) Previous experience reinforcement network for MBON- $\gamma 5\beta'2a$  and MBON- $\gamma 4\gamma 5$ . Both MBONs receive dendritic input in the  $\gamma 5$  compartment but reinforce memories of opposite valence. MBON- $\gamma 4\gamma 5$  provides cross-compartmental feedback innervating PPL1- $\gamma 1pedc$  but not PAM- $\gamma 5$  DANs. MBON- $\gamma 5\beta'2a$  provides feedback to the same compartment  $\gamma 5$  DANs and does not connect to PPL1- $\gamma 1pedc$ . MBON- $\gamma 1pedc > \alpha\beta$  (MVP2) is also part of the network and provides feed-forward inhibition [38]. (D) Key for groups shown in panels E-I. (E-I) Related to Figure 3 E and F. (E-H) Temperature and genetic controls for  $Sh^{\Delta s}$  block during training with sucrose (E and F) and DEET reinforcement (G and H). (I) SEZON activation paired with odor followed by testing 30 min memory replicates the screening phenotypes. SEZON02 produces aversive memories ( $p < 0.0245$ , one-way ANOVA, with Dunnett's post hoc test for multiple comparisons,  $n = 10$ ). (J) Dendrogram of the dendrite of the PPL1- $\gamma 1pedc$  DAN showing upstream MBON presynapses (neato layout - graphviz). All MBON input goes to the CRE branches closest to the axon. MBON- $\gamma 4\gamma 5$  provides the strongest MBON input. (K) Relates to Figure 3G. Clustered input neurons provide selective input to specific branches of the PPL1- $\gamma 1pedc$  DAN dendritic tree.

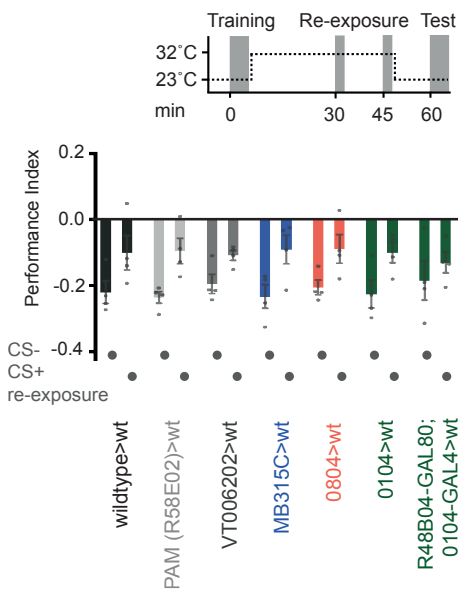
A



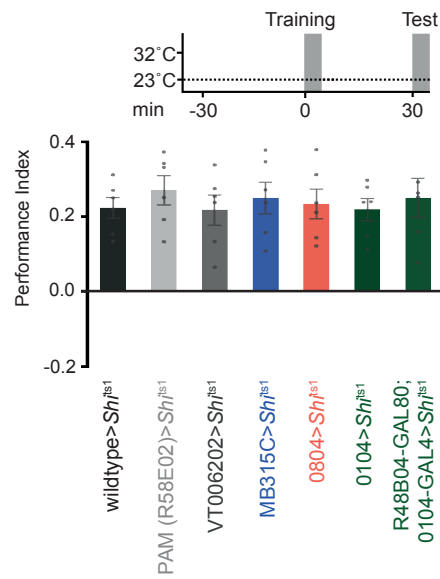
B



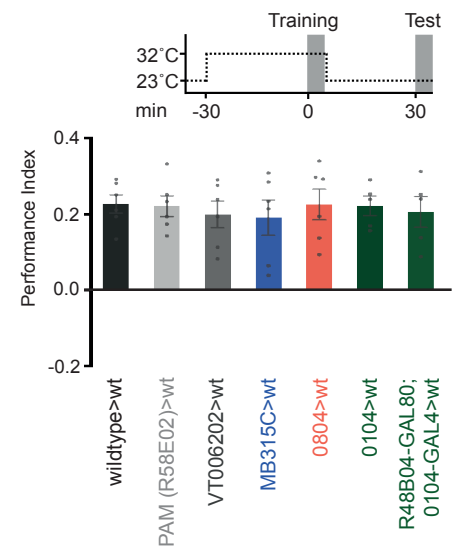
C



D



E



F

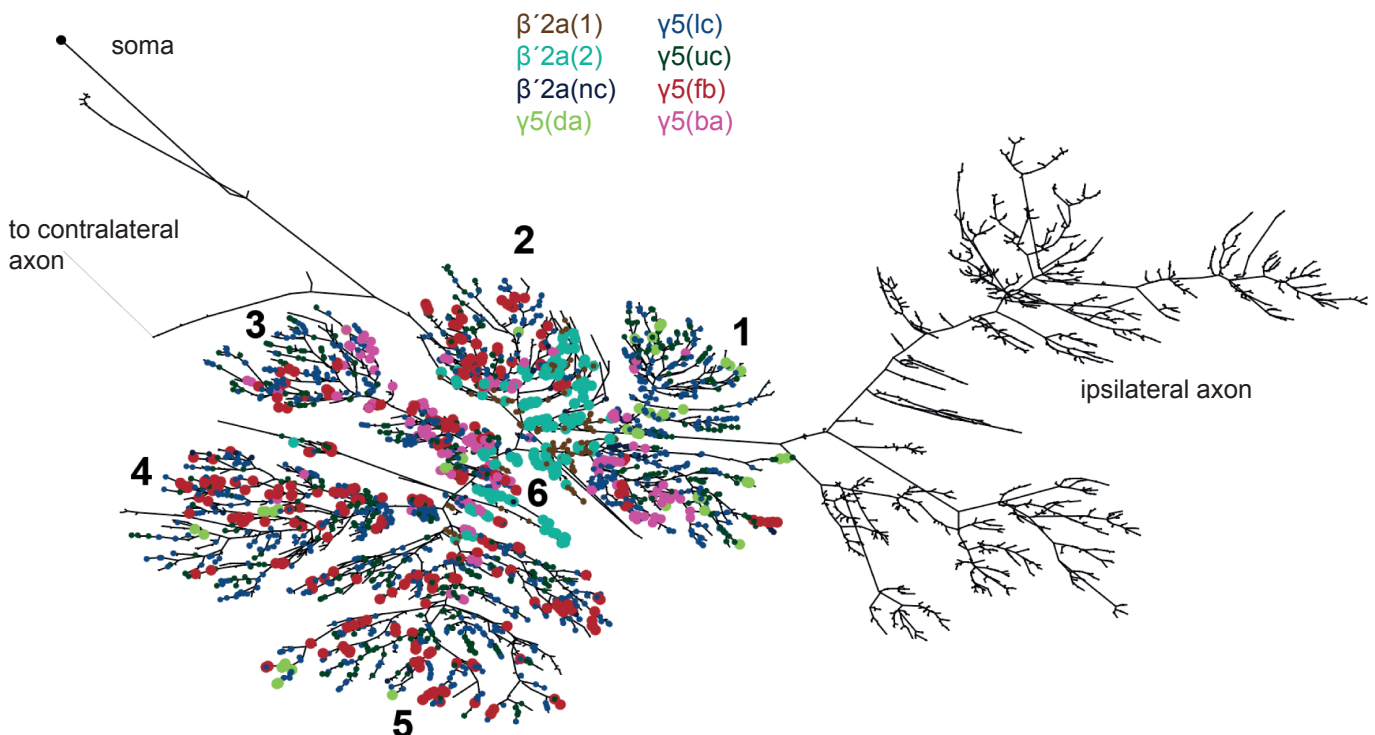


#### Figure S4 related to Figure 4

(A) Dendrograms of two PAM- $\gamma 5(\text{fb})$  DANs with MBON- $\gamma 5\beta'2a$  synaptic inputs shown in green (neato layout - graphviz). MBON- $\gamma 5\beta'2a$  inputs localize close to the root of the dendrite (left) and on a single branch (right). MBON- $\gamma 5\beta'2a$  provides the largest fraction of the postsynaptic budget of  $\gamma 5(\text{fb})$  DANs contributed by a single neuron. (B) Tanglegram showing the correlation between morphological clustering of PAM DAN axons and dendritic connectivity clustering (Pearson's Correlation:  $r=0.292$ ;  $p=0.0006$ ,  $p_w=0.01$  Mantel test). (C) Corresponds to Figure 4F. Heterozygous genetic driver controls show extinction learning ( $n=4$ ). (D) Corresponds to Figure 4G. Permissive temperature control; no defects in 30 min sugar memory were observed ( $n=6$ ). (E) Corresponds to Figure 4G. Genetic driver controls for 30 min sugar memory ( $n=5-6$ ). (F) Dendrogram of MBON- $\gamma 5\beta'2a$  (neato layout - graphviz) with marked MBON postsynapses. Colors correspond to DAN morphology clusters providing the closest presynapse to the MBON postsynapses. We allowed a 2  $\mu\text{m}$  radius around the respective postsynapse to account for dopamine diffusion and assign DAN presynapses. Dendritic branches are numbered 1-6 where 1, 2, and 6 are closest to the root of the dendrite. PAM- $\gamma 5(\text{fb})$ ,  $-\gamma 5(\text{ba})$ ,  $-\gamma 5(\text{da})$ , and  $-\beta'2a$  (2) DANs may influence specific branches, with the  $\gamma 5(\text{da})$  and  $\gamma 5(\text{fb})$  DANs connect exclusive branches and the  $\gamma 5(\text{ba})$  and  $\beta'2a$  (2) inputs localizing very close to the root of the dendrite. Morphologically distinct PAM DANs that receive different inputs might therefore modulate specific branches of the MBON- $\gamma 5\beta'2a$  dendrite.

**Video S1 related to Figure 1A**

3D representations of all canonical RHS DAN skeletons traced to identification in this project within the MB neuropil. PPL1- $\gamma$ 1pedc DAN (red, n=1), PAM- $\gamma$ 5 (green, n=20), PAM- $\beta$ '2a (blue, n=8). Note: for visibility the LHS axonal projections are omitted and only the proximal commissural axons are retained.

**Video S2 related to Figure 1C-1K**

3D representations of skeletons of newly identified subgroups of PAM DANs. Axons from the different subgroups innervate distinct areas in the  $\gamma$ 5 and  $\beta$ '2a compartments and their dendrites occupy unique areas in the SMP. Note: for visibility the LHS axonal projections are omitted and only the proximal commissural axons are retained.

**Video S3 related to Figure 1M**

3D representation of the traced RHS PPL1- $\gamma$ 1pedc DAN skeleton within the MB neuropil. The dendritic arbors are labelled by the different areas of neuropil in which they receive synaptic input: SIP (blue), SMP(violet), dorsal CRE (green), ventral CRE (red). The ipsilateral axon, the soma and soma tract are grey. Video V6 details locations of input from MBONs.

**Video S4 related to Figure 2**

3D representations of the skeletons of 821 neurons that provide input to PPL1- $\gamma$ 1pedc, PAM- $\gamma$ 5 and PAM- $\beta$ '2a DANs. Neurons are shown within the whole brain neuropil color coded according to the first step of coarse clustering (see Star methods for detail). Note: SEZONs are shades of blue, LH-related neurons are shades of yellow, and OTHERS confined to the superior part of the brain are in shades of violet.

**Video S5 related to Figure 3**

3D representation of the skeletons of the fine clusters of input neurons that are studied in detail in this study. Colors correspond to those in Figure 3: LHON01, LHON02, and LHON-AD1b2 neurons are shown in shades of yellow, MBON- $\gamma$ 4 $\gamma$ 5s in green, the RHS MBON- $\gamma$ 5 $\beta$ '2a is coral, SEZONs are shades of blue, and OTHERS are shades of violet.

**Video S6 related to Figure 1M and Figure S3K**

3D representation of the skeleton of the RHS PPL1- $\gamma$ 1pedc DAN within the MB neuropil. The dendritic arbors are labelled by the different areas of neuropil in which they receive synaptic input: SIP (blue), SMP (purple), dorsal CRE (green), ventral CRE (red). The ipsilateral axon, soma and soma tract are grey. The dendritic location of input synapses from MBONs are indicated, with most targeting the CRE portion of the dendritic field. MBON- $\gamma$ 4 $\gamma$ 5 (light blue, 24xCREv + 6xCREd), MBON- $\gamma$ 2 (turquoise, 5xCREd), MBON  $\gamma$ 3 $\beta$ '1 (magenta, 2xCREd + 1xCREv), MBON- $\gamma$ 3 (orange, 2xCREv), MBON- $\gamma$ 2 $\alpha$ '1 (dark blue, 1xCREd), MBON-a3 (red, 1x SMP).